2013

Behavior of hybrid FRP-concrete-steel double-skin tubular columns with a square outer tube and a circular innert tube subjected to axial compression

Tao Yu
University of Wollongong, taoy@uow.edu.au

J G. Teng
Hong Kong Polytechnic University

Publication Details

Yu, T. & Teng, J. G. (2013). Behavior of hybrid FRP-concrete-steel double-skin tubular columns with a square outer tube and a circular innert tube subjected to axial compression. Journal of Composites for Construction, 17 (2), 271-279.

Behavior of hybrid FRP-concrete-steel double-skin tubular columns with a square outer tube and a circular innert tube subjected to axial compression

Abstract
Hybrid fiber-reinforced polymer (FRP) concrete steel, double skin tubular columns (DSTCs) are a new form of hybrid columns. The most common sectional form of hybrid DSTCs consists of a layer of concrete sandwiched between a circular inner steel tube and a circular outer FRP tube whose fiber directions are close to the hoop detection to provide effective confinement to the concrete. Much recent research has been conducted on circular hybrid DSTCs, which has demonstrated that the combination of the three constituent materials leads to several advantages not available with existing forms of columns. In practical applications, for aesthetic and other reasons, square hybrid DSTCs may be needed. This paper thus extends the existing work on circular hybrid DSTCs to square hybrid DSTCs in which the outer FRP tube is square while the inner steel tube is still circular. Results from a series of axial compression tests are presented and interpreted to examine the compressive behavior of square hybrid DSTCs. In these tests, FRP tubes formed through a wet-layup process were used instead of filament-wound FRP tubes because the latter were not readily available to the authors at the time of the study. The test results show that the concrete in these square hybrid DSTCs is effectively confined by the two tubes, and the behavior of the confined concrete is similar to that of concrete in FRP-confined solid columns. A stress-strain model for concrete in square hybrid DSTCs is also proposed and is shown to provide reasonably accurate predictions of the test results. DOI: 10.1061/(ASCE)CC.1943-5614.0000331. (C) 2013 American Society of Civil Engineers.

Keywords
skin, double, steel, concrete, frp, hybrid, behavior, columns, square, outer, tube, tubular, circular, compression, subjected, axial, innert

Disciplines
Engineering | Science and Technology Studies

Publication Details
Yu, T. & Teng, J. G. (2013). Behavior of hybrid FRP-concrete-steel double-skin tubular columns with a square outer tube and a circular innert tube subjected to axial compression. Journal of Composites for Construction, 17 (2), 271-279.

Behavior of Hybrid FRP-Concrete-Steel Double-Skin Tubular Columns with a Square Outer Tube and a Circular Inner Tube Subjected to Axial Compression

T. Yu[1] and J. G. Teng, M.ASCE[2]

Abstract: Hybrid fiber-reinforced polymer (FRP) concrete steel, double skin tubular columns (DSTCs) are a new form of hybrid columns. The most common sectional form of hybrid DSTCs consists of a layer of concrete sandwiched between a circular inner steel tube and a circular outer FRP tube whose fiber directions are close to the hoop detection to provide effective confinement to the concrete. Much recent research has been conducted on circular hybrid DSTCs, which has demonstrated that the combination of the three constituent materials leads to several advantages not available with existing forms of columns. In practical applications, for aesthetic and other reasons, square hybrid DSTCs may be needed. This paper thus extends the existing work on circular hybrid DSTCs to square hybrid DSTCs in which the outer FRP tube is square while the inner steel tube is still circular. Results from a series of axial compression tests are presented and interpreted to examine the compressive behavior of square hybrid DSTCs. In these tests, FRP tubes formed through a wet-layup process were used instead of filament-wound FRP tubes because the latter were not readily available to the authors at the time of the study. The test results show that the concrete in these square hybrid DSTCs is effectively confined by the two tubes, and the behavior of the confined concrete is similar to that of concrete in FRP-confined solid columns. A stress-strain model for concrete in square hybrid DSTCs is also proposed and is shown to provide reasonably accurate predictions of the test results. **DOI: 10.1061/(ASCE)CC.1943-5614.0000331.**

CE Database subject headings: Columns; Fiber reinforced polymer; Confinement; Concrete; Steel; Compression; Hybrid methods.

Author keywords: Hybrid columns; Tubular columns; Confinement; Fiber-reinforced polymer (FRP); Concrete; Steel; Square columns.

Introduction

Over the past two decades, strengthening of structures using bonded fiber-reinforced polymer (FRP) reinforcement has become increasingly popular (Teng et al. 2002; Hollaway and Teng 2008). In addition, extensive research has explored the use of FRP composites in new construction (e.g., Fam and Rizkalla 2001a, b; Mirmiran 2003; Burgueno et al. 2004; Nordin and Taljsten 2004; Fam et al. 2005), in which the combined use of FRP with other materials to create hybrid structures has emerged as a very promising direction (Mirmiran 2003).

Hybrid FRP-concrete-steel double-skin tubular columns (referred to as hybrid DSTCs) are a new form of hybrid columns (Teng et al. 2004, 2007). A hybrid DSTC consists of a layer of concrete sandwiched between an outer tube made of FRP and an inner tube made of steel. In a hybrid DSTC, the FRP tube offers mechanical resistance primarily in the hoop direction to confine the concrete and to enhance the shear resistance of the member; the steel tube acts as the main longitudinal reinforcement and prevents the concrete from inward spalling. The two tubes (i.e., the FRP tube and the steel tube) may be concentrically placed to produce a section form more suitable for columns, or eccentrically placed to produce a section form more suitable for beams (Teng et al. 2007). Hybrid DSTCs may be constructed in situ or precast, with the two tubes acting as the stay-in-place form. Shear connectors should be provided between the steel tube and the concrete, particularly in situations in which bending dominates; such shear connectors are generally not needed between the concrete and the FRP tube if the FRP tube has only a small longitudinal stiffness. This new form of hybrid members represents an innovation that combines the advantages of all three constituent materials and those of the structural form of DSTCs to deliver excellent structural and durability performance.

In the most common sectional form of hybrid DSTCs, both tubes are circular [Fig. 1(a)]; such hybrid DSTCs are referred to in this paper as circular hybrid DSTCs. A large amount of research has recently been completed at The Hong Kong Polytechnic University (PolyU) on circular hybrid DSTCs [Fig. 1(a)] (Teng et al. 2007; Yu et al. 2006, 2010a, b, c, d; Yu 2007; Wong et al. 2008). Teng et al. (2007) explained in detail the rationale for the new member form together with its expected advantages and presented preliminary experimental results to demonstrate some of these advantages, such as excellent ductility and shear resistance. Yu et al. (2006) presented the results of a systematic experimental study on the flexural behavior of hybrid DSTCs and results from a corresponding section analysis following the so-called fiber element approach. Yu et al. (2006) showed that the flexural response of hybrid DSTCs, including their flexural stiffness, cracking load, and ultimate load, can be substantially improved by shifting the inner steel tube toward the tension zone or by providing FRP bars

[1]Lecturer, School of Civil, Mining & Environmental Engineering, Faculty of Engineering, Univ. of Wollongong, Northfields Ave., Wollongong, NSW 2522, Australia.

[2]Chair Professor of Structural Engineering, Dept. of Civil and Structural Engineering, The Hong Kong Polytechnic Univ., Hong Kong, China (corresponding author). E-mail: cejgteng@polyu.edu.hk

Note. This manuscript was submitted on September 29, 2011; approved on September 7, 2012; published online on September 10, 2012. Discussion period open until September 1, 2013; separate discussions must be submitted for individual papers. This paper is part of the ***Journal of Composites for Construction***, Vol. 17, No. 2, April 1, 2013. © ASCE, ISSN 1090-0268/2013/2-271-279/$25.00.

as additional longitudinal reinforcement. Wong et al. (2008) presented a systematic experimental study on the compressive behavior of circular hybrid DSTCs to gain a good understanding of the behavior of concrete in such DSTCs. Yu et al. (2010c, d) developed a new plastic-damage model for FRP-confined concrete and, consequently, a finite-element model for hybrid DSTCs on the basis of the new plastic-damage model (Yu et al. 2010d). On the basis of the available experimental observations and the results from the finite-element model, Yu et al. (2010b) proposed a design-oriented stress-strain model for the confined concrete in circular hybrid DSTCs subjected to axial compression. Yu et al. (2010a) presented experimental results on the behavior of hybrid DSTCs subjected to eccentric compression and a so-called variable confinement model for the confined concrete to account for the effect of strain gradient on confinement effectiveness. These studies at PolyU have led to a simple design approach for circular hybrid DSTCs as columns under concentric or eccentric compression, and this design approach has been adopted by the Chinese code GB50608 (China Planning Press 2010). In addition to research carried out at PolyU, work has also been undertaken by Xu and Tao (2005), Yu (2006), Liu (2007), and Han et al. (2010). These studies have further confirmed some of the performance advantages of hybrid DSTCs under different loading conditions.

Although circular hybrid DSTCs are attractive as bridge piers, square hybrid DSTCs may be preferred if such columns are used in buildings because of aesthetic and other reasons. Hybrid DSTCs, because of their excellent seismic resistance under high axial compression (Liu 2007; Zhang et al. 2012), are very attractive as columns for the lower stories of a tall building. A good understanding of square hybrid DSTCs also provides the necessary basis for future studies on rectangular hybrid DSTCs. This paper therefore presents the first ever study on the axial compressive behavior of square hybrid DSTCs with a square FRP outer tube and a circular steel inner tube [Fig. 1(b)]. A circular inner tube is preferred over a square inner tube because the former provides better confinement to the concrete and is less prone to local buckling. In this paper, results from a series of stub column tests are presented and interpreted, in which the performance of square DSTCs is compared with that of two related column forms, namely, square FRP-confined solid columns (square FCSCs) [Fig. 1(c)] and square FRP-confined hollow columns (square FCHCs) with a circular inner void [Fig. 1(d)]. The purpose of the axial compression tests is twofold: (1) to examine the behavior of square hybrid DSTCs under axial compression and (2) to examine the stress-strain behavior of the confined concrete in the column for the development of a stress-strain model. In these tests, FRP tubes formed through a wet-layup process were used instead of filament-wound FRP tubes because the latter were not readily available to the authors at the time of the study.

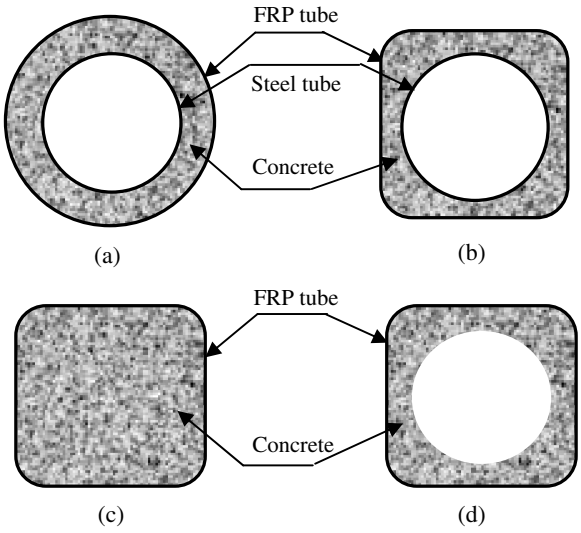

Fig. 1. Cross sections of hybrid DSTCs, FCSCs, and FCHCs: (a) circular hybrid DSTCs; (b) square hybrid DSTCs with a square FRP outer tube and a circular steel inner tube; (c) square FCSCs; (d) square FCHCs with a circular inner void

Axial Compression Tests

Test Specimens

In total, 20 specimens were tested, including 8 DSTC specimens, 4 FCSC specimens, and 8 FCHC specimens. The 8 DSTC specimens included 4 pairs of nominally identical specimens covering 2 different FRP tubes, 2 different steel tubes, and 2 different void area ratios (i.e., ϕ_a, ratio between the area surrounded by the inner circular boundary and that surrounded by the exterior square boundary of the concrete section); the FCSC and the FCHC specimens had the same corresponding dimensions for easy comparison with the DSTC specimens. The present definition of void area ratio differs from the previous definition of void ratio as a diameter ratio [i.e., ϕ, see Wong et al. (2008); Yu et al. (2010a, b)] for circular DSTCs because the latter is inapplicable to the present sectional form. The specimens all had a square outer FRP tube with an inner width of 150 mm, a corner inner radius of 25 mm, and a height of 300 mm. The FRP tubes used in the present study had glass fibers in the hoop direction only and were formed from epoxy resin and unidirectional fiber sheets on the hardened concrete surface using the wet-layup process. These wet-layup FRP tubes were used instead of filament-wound FRP tubes with fiber directions being close to the hoop direction because the latter were not readily available to the authors at the time of the study. Existing tests have shown that there is little difference in behavior between concrete confined by such wet-layup tubes and concrete confined by prefabricated FRP tubes provided their hoop stiffnesses are the same (Mirmiran et al. 1998; Shahawy et al. 2000). Other details of the specimens are summarized in Table 1.

Each specimen is given a name (see Table 1) using the following format: (a) a letter to represent the specimen type (i.e., D for DSTC, S for FCSC, and H for FCHC); (b) a two-digit number to represent the concrete strength; (c) another letter (A or B) to represent the void area ratio (i.e., 0.21 or 0.47) for DSTC and FCHC specimens only; (d) another number to define the number of plies in the FRP tube; and (e) a Roman numeral to differentiate between two nominally identical specimens. For example, specimen D37-B2-II is the

Table 1. Details of Column Specimens

Specimen		FRP tube	Steel tube	Void ratio
Type	Number			
Double skin (DSTC)	D37-A2-I, II	2 plies	Type A	0.21
	D37-A3-I, II	3 plies		
	D37-B2-I, II	2 plies	Type B	0.47
	D37-B3-I, II	3 plies		
Solid (FCSC)	S37-2-I, II	2 plies	—	—
	S37-3-I, II	3 plies		—
Hollow (FCHC)	H37-A2-I, II	2 plies	—	0.21
	H37-A3-I, II	3 plies		
	H37-B2-I, II	2 plies	—	0.47
	H37-B3-I, II	3 plies		

J. Compos. Constr. 2013.17:271-279.

second DSTC specimen of a pair that had a two-ply FRP tube, a void area ratio of 0.47, and a concrete cylinder compressive strength of 37 MPa.

Material Properties

Tensile tests of six FRP flat coupons were conducted, and the testing procedure was consistent with ASTM D7675/D7675M (ASTM 2010). These tests showed that the FRP used had an average maximum tensile force per unit width of 310.3 N/mm per ply and an average tensile stiffness per unit width of 13.6 kN/mm per ply in the direction of fibers. All the column specimens used concrete of the same batch. The concrete was prepared with ordinary portland cement, river sand, and granite aggregate with a maximum nominal size of 10 mm; the water-to-cement ratio of the concrete was 0.6. Three plain concrete cylinders of 152.5 mm in diameter and 305 mm in height were tested to determine the properties of the concrete. The elastic modulus, compressive strength, and compressive strain at peak stress of the concrete averaged from the concrete cylinder tests were 32.8 GPa, 37.5 MPa, and 0.00309, respectively. Tensile tests of three steel coupons were conducted for each type of steel tubes. The coupons were cut from a steel tube along the longitudinal direction and were tested following BS 18 (British Standards Institution 1987). The average values of the outer diameter (D_o), wall thickness (t), elastic modulus (E), yield strength (f_y), and tensile strength (f_u) for each type of steel tubes are listed in Table 2.

Preparation of Specimens

As explained previously, the FRP tubes had fibers in the hoop direction only and were formed through a wet-layup process on the hardened concrete cylinders for all the specimens (Teng et al. 2007), with an overlapping zone of 75 mm on one of the four flat sides of the tubes (Fig. 2).

Test Setup and Instrumentation

For each specimen, four bidirectional strain gauges (BSG1 to BSG4) with a gauge length of 20 mm (Fig. 2) were installed at the four corners of the midheight section of the FRP tube. For the DSTC specimens, additional strain gages were installed: of the two nominally identical DSTC specimens in a pair, one was provided with four additional hoop strain gauges (i.e., SG1 to SG4 in Fig. 2) on the four flat sides of the FRP tube, whereas the other was provided with two additional bidirectional strain gauges with a gauge length of 10 mm (i.e., BSG5 and BSG6 in Fig. 2) at the midheight of the inner steel tube. The circumferential layout of the strain gauges is shown in Fig. 2, in which the overlapping zone is seen to span a circumferential distance of 75 mm.

In addition, two linear variable displacement transducers (LVDTs) were employed to measure the axial shortenings of two opposite sides (i.e., corresponding to SG1 and SG3, respectively, in Fig. 2) of each specimen. All the compression tests were carried out using an MTS machine with a displacement control rate of 0.18 mm/min. All the test data, including strains, loads, and displacements, were recorded simultaneously by a data logger.

Table 2. Measured Properties of Steel Tubes

Steel tube	D_o (mm)	t (mm)	E (GPa)	f_y (MPa)	f_u (MPa)
Type A	76.3	3.3	206.9	364.3	433.1
Type B	114.5	5.2	199.0	381.7	426.9

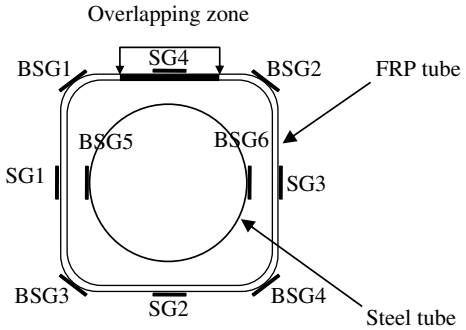

Fig. 2. Layout of strain gauges

Test Results and Discussions

General

All the DSTC and FCSC specimens failed by the rupture of the FRP tube at or near one of the corners as a result of hoop tension. Specimen D37-B2-II after the test is shown in Fig. 3. All the DSTC and FCSC specimens displayed a large deformation capacity before ultimate failure (Figs. 4 and 5). The axial load-shortening responses

Fig. 3. Specimens after test

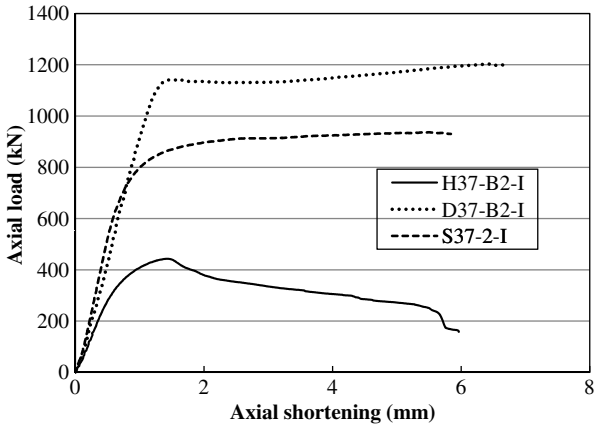

Fig. 4. Typical axial load-shortening curves

J. Compos. Constr. 2013.17:271-279.

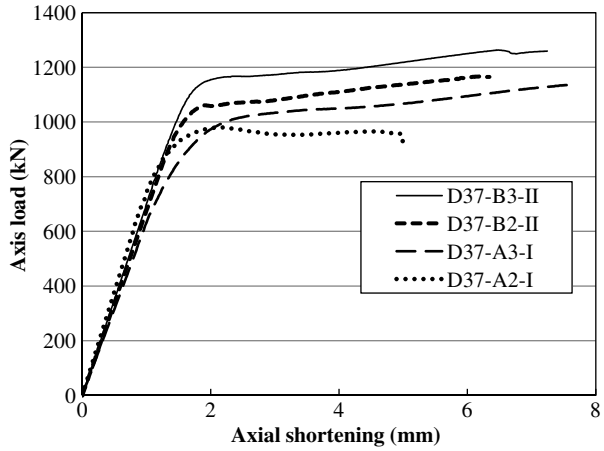

Fig. 5. Typical axial load-strain curves of DSTCs

of these two types of specimens (i.e., DSTC and FCSC specimens) were similar in nature. In the later stage of deformation, the load increased slowly or remained nearly constant.

By contrast, the FCHC specimens behaved quite differently. For all the FCHC specimens, after reaching the peak load, the load decreased significantly before ultimate failure by delamination of the FRP tube (for specimen H37-B2-II) or rupture of the FRP tube (for all the other FCHC specimens). The process of FRP tube rupture was also found to be less explosive and more localized than that of DSTC and FCSC specimens. Specimen H37-B2-II after the test is also shown in Fig. 3. A comparison of typical axial load-shortening curves of the three types of columns is shown in Fig. 4, in which the axial shortening was averaged from the readings of the two LVDTs. In this paper, the following sign convention is adopted: compressive loads, stresses, and strains are positive, whereas tensile strains are negative.

Table 3. Key Test Results of DSTC Specimens

Specimen	P_c (kN)	Average P_c (kN)	P_s (kN)	P_{co} (kN)	$P_c/(P_{co}+P_s)$
D37-A2-I	981	948	323	652	0.97
D37-A2-II	916				
D37-A3-I	1,135	1,142			1.17
D37-A3-II	1,149				
D37-B2-I	1,203	1,185	739	438	1.01
D37-B2-II	1,166				
D37-B3-I	1,309	1,286			1.09
D37-B3-II	1,263				

Behavior of DSTC Specimens

Axial Load–Axial Shortening Behavior

The key test results of all eight DSTC specimens are summarized in Table 3. In this table, P_c is the experimental ultimate load of the DSTC, and fThese hollow steel tubes were tested under axial compression using the same MTS machine with a displacement control DSTCs. These hollow steel tubes were tested under axial compression using the same MTS machine with a displacement control rate of 0.18 mm/ min, and all failed by outward local buckling near one of the tube ends. The average ultimate axial load of each pair of steel tubes (P_s) is listed in Table 3, and the average ultimate axial strains are 0.024 for Type A steel tubes and 0.023 for Type B steel tubes, respectively. The ultimate experimental axial strain (the strain at the rupture or delamination of the FRP tube) was averaged from the readings of the four axial strain gauges at the midheight of the FRP tube and is denoted by ε_{cu} in Table 4. In the same table, the strain of unconfined concrete at peak axial stress averaged from three concrete cylinder tests is denoted by ε_{co} and is used to normalize the experimental ultimate axial strain. For comparison, the nominal ultimate axial strain $\varepsilon_{\mathrm{cu,nom}}$, equal to the ultimate axial shortening averaged from the two LVDTs divided by the specimen height (i.e., 300 mm), is also listed in Table 4.

Table 4. Peak Concrete Stress and Ultimate Strain of All Column Specimens

Specimen	$\sigma_{\max}$ (MPa)	Average $\sigma_{\max}$ (MPa)	$\sigma_{\max}/f_{co}$	ε_{cu}	Average ε_{cu}	$\varepsilon_{cu}/\varepsilon_{co}$	$\varepsilon_{cu,\mathrm{nom}}$	Average $\varepsilon_{cu,\mathrm{nom}}$	$\varepsilon_{cu,\mathrm{nom}}/\varepsilon_{co}$
D37-A2-I	37.8	35.9	0.96	0.0147	0.0125	4.05	0.0176	0.0171	5.53
D37-A2-II	34.1			0.0103			0.0165		
D37-A3-I	46.7	47.1	1.26	0.0226	0.0222	7.18	0.0251	0.0236	7.64
D37-A3-II	47.5			0.0218			0.0220		
D37-B2-I	39.8	38.2	1.02	0.0219	0.0229	7.41	0.0223	0.0222	7.09
D37-B2-II	36.7			0.0238			0.0220		
D37-B3-I	48.9	46.9	1.25	N/A[a]	0.0272[b]	8.80[b]	0.0261	0.0272	8.80
D37-B3-II	45.0			0.0272			0.0282		
S37-2-I	42.6	41.1	1.10	0.0130	0.0130	4.21	0.0194	0.0173	5.60
S37-2-II	39.6			0.0130			0.0151		
S37-3-I	45.3	46.7	1.25	0.0219[c]	0.0225	7.28	0.0211	0.0213	6.89
S37-3-II	48.0			0.0231[c]			0.0215		
H37-A2-I	40.5	39.9	1.06	0.0173	0.0157	5.08	0.0145	0.0145	4.69
H37-A2-II	39.3			0.0141			0.0144		
H37-A3-I	42.6	42.8	1.14	0.0138	0.0128	4.14	0.0179	0.0184	5.95
H37-A3-I	42.9			0.0118			0.0188		
H37-B2-I	40.0	40.6	1.08	0.0179	0.0127	4.12	0.0183	0.0172	5.57
H37-B2-II	41.2			0.00758			0.0160		
H37-B3-I H37-B3-II	39.8	42.4	1.13	0.0139	0.0114	3.70	0.0177	0.0186	6.02
H37-B3-II	44.9			0.00895			0.0194		

Note: N/A = not available.
[a]Most strain gauges had been damaged at the ultimate state.
[b]Results from one specimen only.
[c]One or two strain rosettes were damaged during loading, so the values were averaged from two strain rosettes attached at the two opposite corners.

J. Compos. Constr. 2013.17:271-279.

Table 3 shows that the average ultimate load of the two-ply DSTC specimens is almost the same as the sum of those of the constituent parts, whereas that of the three-ply DSTC specimens is significantly larger than this sum because of the larger circumferential stiffness of the three-ply FRP tubes. The ultimate axial strain of all the DSTC specimens is significantly larger than and is up to approximately nine times that of unconfined concrete (Table 4).

Typical axial load–axial shortening curves of the DSTC specimens are shown in Fig. 5. These curves indicate that the DSTC specimens all had a bilinear load-shortening curve or an almost elastic, perfectly plastic load-shortening curve with large ductility. When all other parameters are the same, the second linear portion of the curve is higher for a specimen with a thicker FRP tube.

Buckling Behavior of the Inner Steel Tube

Because of the existence of the external concrete, the inner steel tube was restrained against local buckling outward. As a result, it is much more difficult for local buckling to occur in the steel tube. In all the DSTC specimens, local buckling deformations had not appeared in the steel tube even at the ultimate state of the specimen. The ultimate axial strains of three-ply DSTCs are similar to or larger than the strain at the ultimate axial load of the hollow steel tubes. Considering that significant outward local buckling deformations of hollow steel tubes were observed at their respective ultimate loads, it can be concluded that the external concrete suppressed the occurrence of local buckling in the steel tube in these DSTC specimens.

Comparison between DSTCs and FCHCs

Typical axial load-shortening curves of the FCHC specimens are shown in Fig. 6. Different from those of the DSTC specimens, the curves of all the FCHC specimens have a clearly descending branch before ultimate failure by the rupture or delamination of the FRP tube. The ultimate failure point can be easily identified from the curves (Fig. 6) because it corresponds to an abrupt increase in the rate of load reduction on these curves. Fig. 6 also shows that while a thicker FRP tube leads to a significantly higher curve for FCHCs with a small void area ratio (i.e., specimens H37-A2-I and H37-A3-I), this effect is not obvious for FCHCs with a relatively large void area ratio (i.e., specimens H37-B2-II and H37-B3-I). It is believed that failure of FCHCs with a large void area ratio is more dependent on the local damage and inward spalling of the concrete layer near its inner surface than its outward expansion, and the use of a thicker FRP tube in such FCHCs is less beneficial.

The key test results of all the DSTC and FCHC specimens are summarized in Table 4. In this table, $\sigma_{\max}$ is the peak axial stress of concrete (equal to the peak load resisted by the concrete layer divided by its cross-sectional area), and ε_{cu} and $\varepsilon_{cu,\text{nom}}$ are the axial strains of concrete at the rupture of the FRP tube obtained from the four axial strain gauge readings and the axial shortening, respectively. For DSTC specimens, the peak load resisted by the concrete layer is assumed to be equal to the difference between the peak load of the DSTC specimen and that of the steel tube, with the latter being found from the hollow steel tube tests. The results given in Table 4 confirm that the use of a thicker FRP tube in FCHCs is less beneficial than in DSTCs in terms of both the peak axial stress and the ultimate axial strain.

Clearly, the performance of DSTCs is superior to that of FCHCs in terms of the axial load-shortening behavior, the peak axial stress of concrete, and the energy dissipation capacity. For a more direct comparison, the axial load–axial shortening curve of specimen D37-B2-I is shown against those of the corresponding steel tube and FCHC specimen (i.e., specimen H37-B2-I) and their sum in Fig. 7. Fig. 7 shows that both the ultimate load and the ductility of specimen D37-B2-I are higher than can be found from the simple superposition of the responses of the steel tube and the FCHC specimen, which clearly demonstrates that beneficial interaction existed between the steel tube and the concrete in specimen D37-B2-I. Similar to observations made about circular DSTCs (Wong et al. 2008), in a square DSTC, the steel inner tube can also effectively restrain the inner surface concrete against inward spalling; such spalling is responsible for the significant postpeak loss of resistance of concrete in a square FCHC.

It is shown in Fig. 7 that the initial slope of the sum curve is noticeably larger than that of the curve of the DSTC specimen, although the two slopes are expected to be similar. Careful examination of the test data and the failed specimen revealed that this difference in the initial stiffness was attributable to a small inaccuracy in the preparation of the DSTC specimen: the top end of the steel tube was found to be a little lower than the concrete surface. This small unevenness was eliminated using gypsum during the capping process for the two ends of the specimen to achieve flat

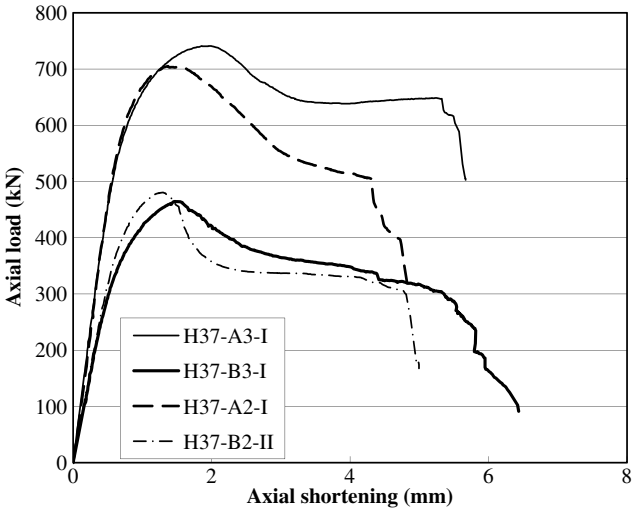

Fig. 6. Axial load-shortening curves of FCHCs

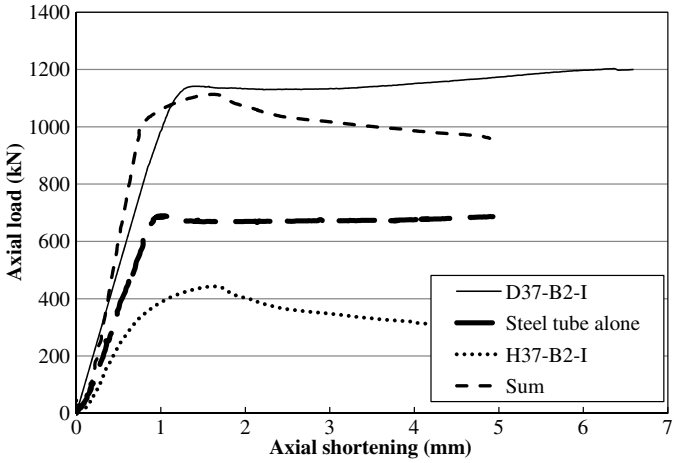

Fig. 7. Comparison between a DSTC specimen and an FCHC specimen

J. Compos. Constr. 2013.17:271-279.

end surfaces. This nonuniform layer of gypsum, being softer than the steel tube, is believed to be the cause of the lower level of strain in the steel tube than the in the concrete (e.g., as a result of local damage in the gypsum layer above the steel tube in the early stage of loading).

Comparison between DSTCs and FCSCs

Fig. 4 shows that the axial load-shortening responses of DSTCs and FCSCs are generally similar in nature: in both cases, the responses indicate approximately linear elastic, perfectly plastic behavior. For a more detailed comparison, the key test results of all the FCSC specimens are also summarized in Table 4. Table 4 shows that for the three-ply specimens, the ultimate axial stress of concrete is almost the same for the two types of columns. For the two-ply specimens, the ultimate axial stress of concrete in the DSTCs is also similar to but slightly smaller than that in the corresponding FCSCs. This small difference is believed to be at least partially attributable to the assumption that the axial load resisted by the concrete layer is equal to the difference between the load resisted by the whole DSTC and that resisted by the steel tube from hollow steel tube tests. One important source of inaccuracy is that the peak loads of the steel tube and the DSTC were probably not reached at the same time in the two-ply DSTCs in which the peak load of the DSTC was reached at a relatively low axial strain (especially for specimens D37-A2-I and II) compared with that at the peak load of the steel tube.

Table 4 also shows that although the DSTCs with a Type A steel tube had almost the same ultimate axial strains as those of the corresponding FCSCs, the ultimate axial strains of the DSTCs with a Type B steel tube (i.e., with a larger void area ratio) are significantly larger than those of the corresponding FCSCs. This observation is similar to that found by Wong et al. (2008) and Yu et al. (2010b) for circular DSTCs. Yu et al. (2010b) concluded that for circular DSTCs, an increase in the ultimate axial strain with the void ratio is attributable to the dependency of the lateral expansion of concrete on the void ratio: in hybrid DSTCs with a larger void area ratio, the lateral expansion is smaller at the same axial strain, leading to a larger ultimate axial strain at hoop rupture failure of an FRP tube with a similar ultimate hoop tensile strain. For further clarification, the axial strain–hoop strain curves of the square DSTC specimens can be compared with those of the corresponding FCSC specimens. A typical comparison for the specimens with a three-ply FRP tube is shown in Fig. 8, in which the hoop strains were averaged from the readings of the four strain gauges at the four corners of the midheight section of the FRP tube and the axial strains were also averaged from readings of these four strain gauges. Fig. 8 confirms that similar to circular DSTCs, the curve of the square DSTC with a smaller void ratio (i.e., specimen D37-A3-II) is almost the same as that of the corresponding square FCSC, but that of the specimen with a larger void ratio (i.e., D37-B3-II) is significantly higher. Yu et al. (2010b) also concluded that the stiffness of the inner steel tube has only a small effect on the behavior of the confined concrete in circular hybrid DSTCs. Further research is necessary to confirm whether this conclusion is also valid for square hybrid DSTCs.

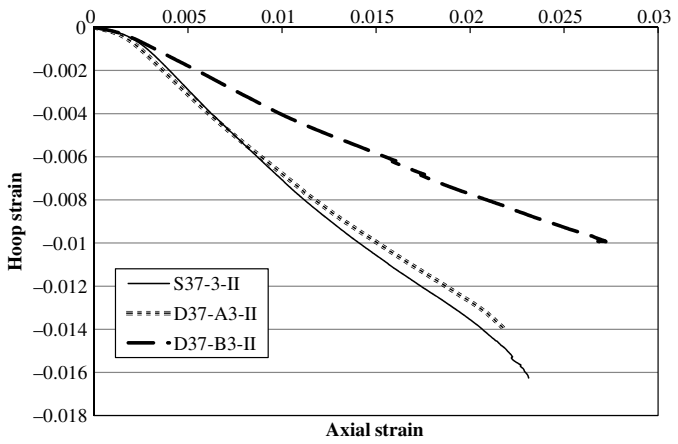

Fig. 8. Axial strain–hoop strain curves

Modeling of Confined Concrete

General

Lam and Teng (2003a) proposed a design-oriented stress-strain model for concrete in circular FCSCs. Two refined versions (Teng et al. 2009) of Lam and Teng's (2003a) model were recently proposed and were shown to provide more accurate predictions than the original model, especially for weakly confined concrete. Yu et al. (2010b) proposed a stress-strain model for concrete in circular hybrid DSTCs, which is based on the model by Teng et al. (2009) and includes modifications to account for the effect of an inner void on the ultimate axial strain of concrete. The model by Yu et al. (2010b) was shown to provide reasonably accurate and conservative predictions of test results.

Lam and Teng (2003b) proposed a stress-strain model for concrete in rectangular (including square) FCSCs on the basis of Lam and Teng's (2003a) model: the equations for the ultimate stress and ultimate axial strain proposed by Lam and Teng (2003a) for circular FCSCs were each modified for application to rectangular FCSCs by including a shape factor. Lam and Teng's (2003b) model was shown to provide satisfactory predictions of the test results available by then and was adopted by the design guideline ACI-440 [American Concrete Institute (ACI) 2008] with some modifications. Subsequently in this section, the present test results of square FCSCs are compared with the predictions of two models: (1) Lam and Teng's (2003b) original model for square FCSCs (referred to as Model A-I) and (2) a refined version of Lam and Teng's (2003b) model for square FCSCs (referred to as Model A-II). Model A-II differs from Model A-I in that the base model for circular FCSCs proposed by Lam and Teng (2003a) is replaced by the refined model of Teng et al. (2009) for circular FCSCs.

On the basis of Model A-I and Model A-II for square FCSCs, two models (referred to as Model B-I and Model B-II, respectively) are also proposed for square DSTCs by incorporating modifications that are the same as those presented in Yu et al. (2010b) to account for the effect of an inner void. Predictions of Model B-I and Model B-II are then compared with the test results of square DSTCs obtained in the present study.

Proposed Stress-Strain Models

On the basis of the previous discussions, Models A-I, A-II, B-I, and B-II for confined concrete are all described by the following expressions:

$$\sigma_c = E_c\varepsilon_c - \frac{(E_c - E_{2c})^2}{4f_o}\varepsilon_c^2 \qquad \text{for } 0 \le \varepsilon_c < \varepsilon_t \tag{1}$$

and

$$\sigma_c = f_o + E_{2c}\varepsilon_c \qquad \text{for } \varepsilon_t \le \varepsilon_c \le \varepsilon_{cu} \tag{2}$$

J. Compos. Constr. 2013.17:271-279.

where σ_c and ε_c = axial stress and axial strain, respectively; E_c = elastic modulus of unconfined concrete; E_{2c} = slope of the linear second portion of the stress-strain curve; f_o = intercept of the stress axis by the linear second portion; and ε_{cu} = ultimate axial strain of confined concrete. The parabolic first portion meets the linear second portion with a smooth transition at ε_t, which is given by

$$\varepsilon_t = \frac{2f_o}{(E_c - E_{2c})} \tag{3}$$

The slope of the linear second portion E_{2c} is given by

$$E_{2c} = \frac{f'_{cc} - f_o}{\varepsilon_{cu}} \tag{4}$$

where f'_{cc} = compressive strength of confined concrete. The value of f_o is assumed to be the compressive strength of unconfined concrete, f'_{co}, in all four models as proposed by Lam and Teng (2003a).

The four models differ only in the equations for the compressive strength f'_{cc} and the ultimate axial strain ε_{cu} of confined concrete. For square FCSCs, Lam and Teng (2003b) proposed Eq. (5) for f'_{cc} and Eq. (6) for ε_{cu} (i.e., Model A-I)

$$\frac{f'_{cc}}{f'_{co}} = \begin{cases} 1 + 3.3k_{s1}f_l/f'_{co} & \text{if } f_l/f'_{co} \geq 0.07 \\ 1 & \text{if } f_l/f'_{co} < 0.07 \end{cases} \tag{5}$$

$$\frac{\varepsilon_{cu}}{\varepsilon_{co}} = 1.75 + 12k_{s2}\left(\frac{f_l}{f'_{co}}\right)\left(\frac{\varepsilon_{h,rup}}{\varepsilon_{co}}\right)^{0.45} \tag{6}$$

In Eqs. (5) and (6), the two shape factors k_{s1} and k_{s2} become identical and are defined by the following equation for square FCSCs without steel reinforcement:

$$k_{s1} = k_{s2} = 1 - \frac{2(b - 2R_c)^2}{3A_g} \tag{7}$$

where A_g = gross area of the column section with rounded corners; b = width of the column section; and R_c = corner radius. The value of f_l is the maximum equivalent confining pressure provided by the FRP tube at rupture failure and is defined by the following equation for square FCSCs (Lam and Teng 2003b):

$$f_l = \frac{\sqrt{2}E_{\text{frp}}t_{\text{frp}}\varepsilon_{h,\text{rup}}}{b} \tag{8}$$

where E_{frp} = elastic modulus of FRP in the hoop direction; t_{frp} = thickness of the FRP tube; and $\varepsilon_{h,\text{rup}}$ = equivalent rupture strain of FRP and is assumed to be the actual hoop rupture strain found from circular specimens confined by the same FRP material (Lam and Teng 2003b).

In Model A-II, Eq. (9) is proposed for f'_{cc}, and Eq. (10) for ε_{cu}

$$\frac{f'_{cc}}{f'_{co}} = \begin{cases} 1 + 3.5k_{s1}(\rho_k - 0.01)\rho_\varepsilon & \text{if } \rho_k \geq 0.01 \\ 1 & \text{if } \rho_k < 0.01 \end{cases} \tag{9}$$

$$\frac{\varepsilon_{cu}}{\varepsilon_{co}} = 1.75 + 6.5k_{s2}\rho_K^{0.8}\rho_\varepsilon^{1.45} \tag{10}$$

where $\rho_K = E_{\text{frp}}t_{\text{frp}}/(E_{\text{sec},o}R_o)$ = confinement stiffness ratio; and $\rho_\varepsilon = \varepsilon_{h,\text{rup}}/\varepsilon_{co}$ = strain ratio.

Models B-I and B-II are for square DSTCs and are based on Models A-I and A-II, respectively. In Model B-I, Eq. (5) is used for f'_{cc}, and the following equation is proposed for ε_{cu}:

$$\frac{\varepsilon_{cu}}{\varepsilon_{co}} = 1.75 + 12k_{s2}\left(\frac{f_l}{f'_{co}}\right)\left(\frac{\varepsilon_{h,\text{rup}}}{\varepsilon_{co}}\right)^{0.45}(1 - \phi)^{-0.22} \tag{11}$$

In Model B-II, Eq. (9) is used for f'_{cc}, and the following equation is proposed for ε_{cu}:

$$\frac{\varepsilon_{cu}}{\varepsilon_{co}} = 1.75 + 6.5k_{s2}\rho_K^{0.8}\rho_\varepsilon^{1.45}(1 - \phi)^{-0.22} \tag{12}$$

In Models B-I and B-II, ϕ is the equivalent void ratio of a square DSTC and is defined as

$$\phi = \sqrt{\phi_a} \tag{13}$$

Other parameters in Models B-I and B-II, including k_{s1}, k_{s2}, and f_l are assumed to be the same as those for a square FCSC with the same FRP tube (i.e., the material properties of and the area of the region surrounded by the FRP tube are the same for both the square FCSC and the square DSTC).

Comparison with Test Results

Predictions of the four models are compared in this section with the present test results. In making the predictions, the equivalent FRP rupture strain was assumed to be 0.0182, which is the average value reported by Jiang and Teng (2007) for circular FCSCs with the same FRP material.

Figs. 9(a and b) show comparisons between the predictions of Models A-I and A-II and the test results of the FCSC specimens. It is evident that the predictions of Model A-I [i.e., Lam and Teng's (2003b) original model] are higher than the experimental curves, with a larger concrete strength and a smaller ultimate axial strain. By incorporating modifications that are the same as those given in Teng et al. (2009) [i.e., Eqs. (9) and (10)], Model A-II provides significantly closer predictions of test results: the predictions are more accurate for the two-ply FCSC specimens than for the three-ply FCSC specimens, and the ultimate axial strain is still significantly underestimated for the latter.

Figs. 9(c–e) show comparisons between the predictions of Models B-I and B-II and the test results of the three DSTC specimens with strain gauges attached on the inner steel tube (in total, four DSTCs had strain gauges on the steel tubes as stated previously, but those on one of the four were unexpectedly damaged). In Figs. 9(c–e), the experimental axial stress of the concrete is defined as the load carried by the concrete layer divided by its cross-sectional area. The load carried by the concrete layer is assumed to be equal to the difference between the load carried by the DSTC specimen and the load carried by the steel tube at the same axial strain. The latter was found from the hollow steel tube test results by making use of axial strain readings from strain gauges installed on the steel tube in hybrid DSTCs. When the axial strain of a DSTC specimen exceeds the buckling strain found from the corresponding hollow steel tube tests, it is assumed that the load resisted by the steel inner tube is equal to P_s; this assumption is reasonable because buckling of the steel tube was prevented by the concrete in the present DSTC specimens. As expected, Model B-II (based on Model A-II) provides closer predictions of the test results than Model B-I (based on Model A-I). Model B-II provides reasonably accurate predictions of the compressive strength of confined concrete, but it still significantly underestimates the experimental ultimate axial strain for specimens with a large void area ratio. This underestimation is believed to be at least partially attributable to the inaccuracy of Model A-II for square FCSCs. Therefore, further research is needed to develop more accurate models for both FCSCs and DSTCs.

J. Compos. Constr. 2013.17:271-279.

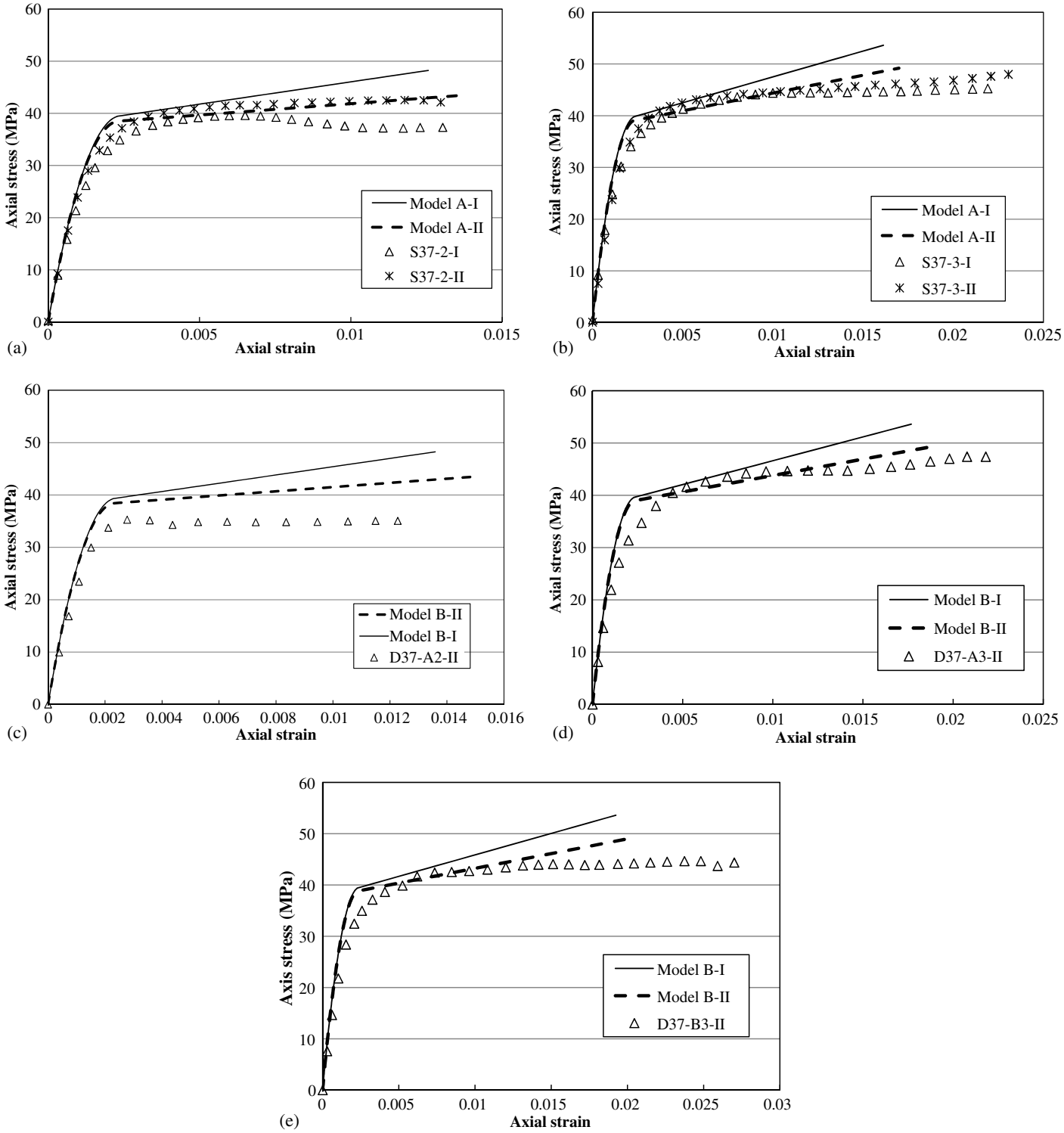

Fig. 9. Axial stress-strain curves: (a) FCSC specimens with a two-ply FRP jacket; (b) FCSC specimens with a three-ply FRP jacket; (c) specimen D37-A2-II; (d) specimen D37-A3-II; (e) specimen D37-B3-II

Conclusions

This paper has presented the results of an experimental study on the axial compressive behavior of hybrid FRP-concrete-steel DSTCs with a square FRP outer tube and a circular steel inner tube. On the basis of the test results and discussions presented in the paper, the following conclusions may be drawn:

1. The concrete in square hybrid DSTCs is effectively confined by the two tubes, and local buckling of the inner steel tube is constrained by the surrounding concrete, leading to a very ductile response. The axial stress-strain behavior of concrete in such DSTCs is very similar to that of concrete in square FCSCs.
2. Square DSTCs are superior to square FCHCs. The inner steel tube plays the important role of preventing the concrete near the inner edge from inward spalling.
3. The ultimate axial stress of concrete in a square DSTC is generally similar to that in a corresponding square FCSC.

J. Compos. Constr. 2013.17:271-279.

The ultimate axial strain of concrete in a square DSTC depends significantly on the void area ratio and may be considerably higher than that of FCSCs with the same FRP tube and concrete strength. Further research is needed to clarify the effect of stiffness of the steel inner tube on both the ultimate axial stress and ultimate axial strain of concrete in square DSTCs.

This paper has also proposed two simple stress-strain models for concrete in hybrid DSTCs on the basis of existing stress-strain models for concrete in FRP-confined circular solid columns, square solid columns, and circular DSTCs. One of the two models, named Model B-II, has been found to provide reasonably accurate predictions of the test results. It has also been pointed out that if the accuracy of the proposed stress-strain model for concrete in DSTCs is to be improved, a more accurate stress-strain model for concrete in square FRP-confined solid columns needs to be developed, as the former is based on the latter.

Acknowledgments

The authors gratefully acknowledge the financial support provided by the Research Grants Council of the Hong Kong Special Administrative Region, China (Project No. PolyU 5278/07E); the Science Technology Department of Zhejiang Province, China (Grant No. 2009C14006); and The Hong Kong Polytechnic University. The authors also wish to thank Miss Chan Pak Yan for her valuable contribution to the experimental work.

References

American Concrete Institute (ACI). (2008). "Guide for the design and construction of externally bonded FRP systems for strengthening concrete structures." *ACI-440*, Committee 440, Detroit, MI.

ASTM. (2010). "Standard test method for determining tensile properties of fiber reinforced polymer matrix composites used for strengthening of civil structures." ASTM D7565/D7565M, Committee D30, West Conshohoken, PA.

British Standards Institution. (1987). "Tensile testing of metals (including aerospace materials)." *BS 18*, London.

Burgueno, R., Davol, A., Zhao, L., Seible, F., and Karbhari, V. M. (2004). "Flexural behavior of hybrid fiber-reinforced polymer/concrete beam/slab bridge component." *ACI Struct. J.*, 101(2), 228–236.

China Planning Press. (2010). "Code for infrastructure application of FRP composites." *GB50608*, Beijing, China.

Fam, A. Z., and Rizkalla, S. H. (2001a). "Behavior of axially loaded concrete-filled circular fiber reinforced polymer tubes." *ACI Struct. J.*, 98(3), 280–289.

Fam, A. Z., and Rizkalla, S. H. (2001b). "Confinement model for axially loaded concrete confined by circular fiber-reinforced polymer tubes." *ACI Struct. J.*, 98(4), 451–461.

Fam, A., Schnerch, D., and Rizkalla, S. (2005). "Rectangular filament-wound GFRP tubes filled with concrete under flexural and axial loading: experimental investigation." *J. Compos. Constr.*, 9(1), 25–33.

Han, L. H., Tao, Z., Liao, F. Y., and Xu, Y. (2010). "Tests on cyclic performance of FRP-concrete-steel double-skin tubular columns." *Thin-Walled Struct.*, 48(6), 430–439.

Hollaway, L. C., and Teng, J. G., eds. (2008). *Strengthening and rehabilitation of civil infrastructures using FRP composites*, Woodhead, Cambridge, U.K.

Jiang, T., and Teng, J. G. (2007). "Analysis-oriented stress-strain models for FRP-confined concrete." *Eng. Struct.*, 29(11), 2968–2986.

Lam, L., and Teng, J. G. (2003a). "Design-oriented stress-strain model for FRP-confined concrete." *Constr. Build. Mater.*, 17(6–7), 471–489.

Lam, L., and Teng, J. G. (2003b). "Design-oriented stress-strain model for FRP-confined concrete in rectangular columns." *J. Reinf. Plast. Compos.*, 22(13), 1149–1186.

Liu, M. X. (2007). "Studies on key behavior of FRP-concrete-steel double skin tubular columns." Ph.D. thesis, Tsinghua Univ., Beijing, China (in Chinese).

Mirmiran, A. (2003). "Stay-in-place FRP form for concrete columns." *Adv. Struct. Eng.*, 6(3), 231–241.

Mirmiran, A., Shahawy, M., Samaan, M., Echary, H. E., Mastrapa, J. C., and Pico, O. (1998). "Effect of column parameters on FRP-confined concrete." *J. Compos. Constr.*, 2(4), 583–590.

Nordin, H., and Taljsten, B. (2004). "Testing of hybrid FRP composite beams in bending." *Compos. Part B: Eng.*, 35(1), 27–33.

Shahawy, M., Mirmiran, A., and Beitelman, T. (2000). "Tests and modeling of carbon-wrapped concrete columns." *Compos. Part B: Eng.*, 31(6–7), 471–480.

Teng, J. G., Chen, J. F., Smith, S. T., and Lam, L. (2002). *FRP-strengthened RC structures*, John Wiley and Sons, West Sussex, U.K.

Teng, J. G., Jiang, T., Lam, L., and Luo, Y. Z. (2009). "Refinement of a design-oriented stress-strain model for FRP-confined concrete." *J. Compos. Constr.*, 13(4), 269–278.

Teng, J. G., Yu, T., and Wong, Y. L. (2004). "Behavior of hybrid FRP-concrete-steel double-skin tubular columns." *Proc., 2nd Int. Conf. on FRP Composites in Civil Engineering*, Taylor & Francis, Melbourne, Australia, 811–818.

Teng, J. G., Yu, T., Wong, Y. L., and Dong, S. L. (2007). "Hybrid FRP-concrete-steel tubular columns: Concept and behavior." *Constr. Build. Mater.*, 21(4), 846–854.

Wong, Y. L., Yu, T., Teng, J. G., and Dong, S. L. (2008). "Behavior of FRP confined concrete in annular section columns." *Compos. Part B: Eng.*, 39(3), 451–466.

Xu, Y., and Tao, Z. (2005). "Key issues of dynamic behavior of hybrid FRP-concrete-steel double skin tubular columns." *J. Fuzhou Univ. (Nat. Sci.)*, 33(S1), 309–315 (in Chinese).

Yu, T. (2007). "Behavior of hybrid FRP-concrete-steel double-skin tubular columns." Ph.D. thesis, The Hong Kong Polytechnic Univ., Hong Kong, China.

Yu, T., Teng, J. G., and Wong, Y. L. (2010a). "Behavior of hybrid FRP-concrete-steel double-skin tubular columns subjected to eccentric compression." *Adv. Struct. Eng.*, 13(5), 961–974.

Yu, T., Teng, J. G., and Wong, Y. L. (2010b). "Stress-strain behavior of concrete in hybrid double-skin tubular columns." *J. Struct. Eng.*, 136(4), 379–389.

Yu, T., Teng, J. G., Wong, Y. L., and Dong, S. L. (2010c). "Finite element modeling of confined concrete-I: Drucker-Prager type plasticity model." *Eng. Struct.*, 32(3), 665–679.

Yu, T., Teng, J. G., Wong, Y. L., and Dong, S. L. (2010d). "Finite element modeling of confined concrete-II: Plastic-damage model." *Eng. Struct.*, 32(3), 680–691.

Yu, T., Wong, Y. L., Teng, J. G., Dong, S. L., and Lam, S. S. (2006). "Flexural behaviour of hybrid FRP-concrete-steel double skin tubular members." *J. Compos. Constr.*, 10(5), 443–452.

Yu, X. W. (2006). "Behavior of hybrid CFRP-concrete-steel double-skin tubular columns under axial compression." M.Sc. thesis, Harbin Institute of Technology, Shenzhen, China (in Chinese).

Zhang, B., Teng, J. G., and Yu, T. (2012). "Behaviour of hybrid double-skin tubular columns subjected to combined axial compression and cyclic lateral loading." *Proc., 6th Int. Conf. on FRP Composites in Civil Engineering*, Rome, Italy, 13–15 June.

J. Compos. Constr. 2013.17:271-279.